Physica Medica 65 (2019) 53–58

Contents lists available at ScienceDirect

Physica Medica

journal homepage: www.elsevier.com/locate/ejmp

Original paper

Availability of a simplified lung ventilation imaging algorithm based on four-dimensional computed tomography

Yuan Tian, Junjie Miao, Zhiqiang Liu, Peng Huang, Wenqin Wang, Xin Wang, Yirui Zhai, Jingbo Wang, Minghui Li, Pan Ma, Ke Zhang, Hui Yan, Jianrong Dai*

Department of Radiation Oncology, National Cancer Center/National Clinical Research Center for Cancer/Cancer Hospital, Chinese Academy of Medical Science and Peking Union Medical College, Beijing 100021, China

ARTICLE INFO

Keywords:
Ventilation image
4DCT
SPECT
Deformable vector field
Dice similarity coefficient

ABSTRACT

Purpose: It is still not conclusive which four-dimensional computed tomography (4DCT)-based ventilation imaging algorithm is most accurate and efficient. In this study, we proposed a simplified algorithm (VIAAVG) which only requires the average computed tomography (AVG CT) as input, and quantitatively compared its accuracy and efficiency with three other popular algorithms.

Material and methods: Fifty patients with lung or esophageal cancer who underwent radiotherapy were enrolled. Single photon emission computed tomography (SPECT) ventilation images (VI-SPECT) and 4DCT were acquired 1–3 days before the first treatment session. The end of exhalation and the end of inhalation CT were registered to derive deformable vector field (DVF) using MIMvista. 4DCT-based ventilation images (CTVI) were first calculated respectively by means of four algorithms (VIAJAC, VIAHU, VIAPRO and VIAAVG). The computation times were compared using paired *t*-test. The corresponding CTVIs (CTVIJAC, CTVIHU, CTVIPRO and CTVIAVG) and VI-SPECT were segmented into three equal sub-volumes (high, medium and low function lung, respectively) after smoothing and normalization. The Dice Similarity Coefficients (DSCs) were calculated for each sub-volume between each CTVI and VI-SPECT. The average DSCs for high, medium and low function lung in different CTVIs for each patient were compared using paired *t*-test.

Results: The mean DSCs for CTVIJAC, CTVIHU, CTVIPRO and CTVIAVG were 0.3255, 0.4465, 0.5865 and 0.5958, respectively. The average computation times for CTVIJAC, CTVIHU, CTVIPRO and CTVIAVG were 18.3 s, 24.2 s, 144.8 s and 15.0 s.

Conclusion: VIAAVG is available for clinical use because of its high accuracy, improved efficiency and less input requirement compared to the other algorithms.

1. Introduction

It is beneficial to utilize pulmonary function images, acquired by single photon emission tomography (SPECT) [1] or positron emission tomography (PET) [2] in radiotherapy. In recent years, four-dimensional computed tomography (4DCT)-based ventilation imaging has become a research hotpot. It can provide functional information in lung without additional dose or monetary cost to the patient, since 4DCT simulation is a clinical routine for thoracic cancer patient in most of radiation oncology clinics. In clinical practice, the 4DCT-based Ventilation Image (CTVI) has been used for assessing the regional function [3] or function changes [4–8] in lung tissue, predicting radiation pneumonitis [9,10] and guiding radiotherapy treatment planning [2,11–15].

Three ventilation imaging algorithms (VIA) to produce CTVI have been reported. The first VIA (VIAHU) is described by Guerrero et al. [16] which generates static 3D ventilation images based solely on the physical density-change between the exhalation breath-hold and inhalation breath-hold computed tomography (CT) images using deformable image registration (DIR) and the underlying CT density information. The second widely used VIA (VIAJAC) is introduced by Reinhardt et al. [17], which utilizes the Jacobian determinant of the DIR spatial transformation to quantify the regional volume-change of lung volume elements. The third VIA (VIAPRO) is proposed by Kipritidis et al. [18], which estimates the ventilation in terms of the 4D time-averaged regional product of air and tissue densities at each voxel without requiring DIR.

However, the correlations between the CTVIs based on any of above

* Corresponding author.
E-mail address: dai_jianrong@cicams.ac.cn (J. Dai).

https://doi.org/10.1016/j.ejmp.2019.08.006
Received 18 January 2019; Received in revised form 8 July 2019; Accepted 5 August 2019
Available online 12 August 2019

algorithms and the clinical golden standard (^{99m}Tc-SPECT [19] or ^{68}Ga-Galligas PET [20]) are highly variable [21–24]. Many causes have been reported, such as the image quality [25], breathing variations [26], the DIR inaccuracy [27,28], and the 4DCT sorting method [29]. It still remains unclear which VIA is the most accurate and efficient for clinical use.

Inspired by the study of Kipritidis et al. [18], in this study we propose a simplified VIA (VIAAVG) , which requires only average CT (AVG CT) as input data. Its availability is quantitatively evaluated by comparing the accuracy and efficiency of VIAAVG with those VIAs proposed before (i.e. VIAHU, VIAJAC and VIAPRO) for 50 enrolled patients.

2. Material and methods

2.1. Patients

Fifty thoracic cancer patients (lung or esophageal cancer) were enrolled in this study and underwent radiotherapy in our hospital between 2015 and 2018. 4DCT images were acquired in 4DCT simulation as routine part of radiotherapy prior to the treatment. SPECT ventilation images (VI-SPECT) were also acquired 1–3 days before the first radiotherapy session with the same supine position used in 4DCT simulation. The time interval between 4DCT simulation and VI-SPECT acquisition was less than 3 days to ensure the lung function of patient stayed consistent without any therapeutics and drug intervention. The research protocol was approved by the Clinical Research Committee and the Ethics Committee at the Cancer Hospital, Chinese Academy of Medical Science. In Table 1, the patient characteristics are reported.

2.2. 4DCT acquisition

Free-breathing 4DCT was acquired with patients in a supine position using a Brilliance Bigbore CT scanner (Philips Healthcare, Andover, MA) with no i.v. contrast. For each patient, 4DCT images of the entire target and thorax, as well as upper abdomen were obtained. Real-time Positioning Management (RPM, Varian Medical Systems, Palo Alto, CA) was used for respiratory monitoring. The entire respiratory cycle was recorded and divided into ten equal temporal phases, defining the peak-inhalation phase as T00 and peak-exhalation phase as T50 [30]. The raw data was sorted into corresponding phase bins and reconstructed into ten phase CT datasets (T00-T90, respectively) with the dimension of 512 × 512 and 5 mm slice thickness. AVG CT was reconstructed from 10-phase 4DCT data relating to the percentage of time with the same spatial resolution and used as the planning CT (pCT). Hence, no displacement existed between all phases of 4DCT and pCT.

2.3. VI-SPECT acquisition

Each patient received ventilation SPECT in the same supine position on a dual head Discovery NM 670 SPECT/CT system (GE Healthcare, Milwaukee, WI). ^{99m}Tc-Technegas (Cyclomedica Australia Pty Ltd), an ultra-fine suspension of carbon nanoparticles labeled with technetium was inhaled into the resting tidal breathing patient to ensure 30 MBq of activity within the lungs. SPECT acquisitions were performed using 3° steps through a 360° acquisition and 20 s per view (according to 20 min acquisition time). A low-dose CT was also acquired by the same system in the same session to perform attenuation correction of the ^{99m}Tc 140 keV emission photons. Ventilation SPECT data were reconstructed in a 64x64 matrix using the proprietary 3D ordered subsets expectation maximization (OSEM) algorithm.

Table 1
Clinical parameters for the patient population enrolled in the study.

Parameter	Median (range) or number (%)
Age	62 (36–78)
Sex	Male 40 (80%)/Female 10 (20%)
Tumor	Lung cancer 20 (40%)/Esophageal cancer 30 (60%)
COPD	YES 2 (4%)/NO 48 (96%)
Smoking status	YES 35 (70%)/NO 15 (30%)
Tumor stage	I 0 (0%)/II 4 (8%)/III 32 (64%)/IV 14 (28%)

Note: COPD is the abbreviation as 'chronic obstructive pulmonary disease'.

2.4. Registration between VI-SPECT and pCT

VI-SPECT and the pCT were registered using two-steps strategy in order to improve the registration accuracy. First, the low-dose CT was rigidly registered to the pCT using MIMvista 6.0 (MIM Software Inc., Cleveland, OH), a commercial software used for deformable registration without user defined parameters. The registration was validated by an experienced radiation oncologist. Then, the displacement between low-dose CT and pCT was directly used to correct the position mismatch between VI-SPECT and pCT considering the changes in body morphology between the VI-SPECT and low-dose CT scans were minimized because they are performed by the same system in the same session. The registered VI-SPECT was interpolated into the same spatial resolution with pCT (i.e. 512 × 512 and 5 mm slice thickness) using MIMvista.

2.5. Binary lung mask generation

The lung volume was contoured on each CT phase using threshold-based approach with intensity cutoff between −250 HU and −1000 HU in MIMvista. Central airway and great vessels where the ^{99m}Tc-Technegas physiologically concentrated were manually trimmed to define the region of interest for comparison. The lung volume was transformed into a 3D binary mask in which the value of voxel inside and outside the lung was set equal to 1 and 0, respectively.

2.6. DIR between T00 and T50

DIR was performed to link each lung voxel elements from the T00 to the T50 using MIMvista. No user-defined parameters were used in order to avoid the influence of user-defined parameters on the registration accuracy. The deformable vector fields (DVFs), which defined the spatial correspondence of HUs between T00 and T50, were exported with the same dimension as pCT and then used for the computation of the DIR-dependent CTVIs (CTVIHU and CTVIJAC).

Binary lung masks, DVFs, ten phases of 4DCT (T00, …, T90) and AVG CTs were saved as matrices by mean of an in-house image toolkit called FLICT (i.e. Functional Lung Image based on 4DCT toolkit) developed with MATLAB (Mathworks Inc.) interface. These data would be used as input for subsequent ventilation image computation with different VIAs. The VI-SPECTs after registration and interpolation were also saved by FLICT and used as the standard for comparing the accuracy of different VIAs.

2.7. Computation of CTVIHU

The density-based specific ventilation, CTVIHU, was derived by the following expression proposed by Castillo et al. [23] in term of registered CT numbers corresponding to inhalation and exhalation breathing states:

$$CTVIHU = 1000\frac{(H_{T00}^{VOI} - HU_{T50})}{HU_{T50}(1000 + H_{T00}^{VOI})} \quad (1)$$

where HU_{T50} was the HU value of voxel in the peak exhalation phase CT (i.e. T50), and H_{T00}^{VOI} was the average of all HU corresponding to the set of T00 voxels that mapped into the T50 voxels under consideration.

2.8. Computation of CTVIJAC

The jacobian-based specific ventilation (CTVIJAC) was derived by quantifying the regional volume-change of lung volume elements with the Jacobian determinant of the DVFs. This method was used in Kida et al. study [15]:

$$\mathrm{CTVIJAC} = \mathrm{J} - 1 \tag{2}$$

where J was the regional volume change calculated from the Jacobian determinant of DVFs:

$$\mathrm{J} = \begin{vmatrix} 1 + \frac{\partial \mathrm{DVF_x}}{\partial x} & \frac{\partial \mathrm{DVF_x}}{\partial y} & \frac{\partial \mathrm{DVF_x}}{\partial z} \\ \frac{\partial \mathrm{DVF_y}}{\partial x} & 1 + \frac{\partial \mathrm{DVF_y}}{\partial y} & \frac{\partial \mathrm{DVF_y}}{\partial z} \\ \frac{\partial \mathrm{DVF_z}}{\partial x} & \frac{\partial \mathrm{DVF_z}}{\partial y} & 1 + \frac{\partial \mathrm{DVF_z}}{\partial z} \end{vmatrix} \tag{3}$$

2.9. Computation of CTVIPRO

CTVIPRO was calculated in terms of the 4D time-averaged regional product of air and tissue densities at each voxel, based on the method proposed by Kipritidis et al. [18]:

$$\mathrm{CTVIPRO}(x) = \sum_{1}^{N} V_{\varnothing}(x)/N \tag{4}$$

where:

$$V_{\varnothing}(x) = \begin{cases} f_{\varnothing}^{\mathrm{Air}}(x) \times f_{\varnothing}^{\mathrm{Tissue}}(x) & \text{if } x \in L_{\varnothing} \\ 0 & \text{if } x \notin L_{\varnothing} \end{cases} = \begin{cases} \frac{HU_{\varnothing}(x)}{-1000} \times \frac{HU_{\varnothing}(x)+1000}{1000} & \text{if } x \in L_{\varnothing} \\ 0 & \text{if } x \notin L_{\varnothing} \end{cases} \tag{5}$$

Here, $HU_{\varnothing}(x)$ was the HU value at voxel × and φ was the 4DCT phase bin (T00, T10, … , T90). L_{φ} was the binary lung mask defined on each phase CT.

2.10. Computation of CTVIAVG

As indicated in Eq. (5), all phases of 4DCT and the corresponding binary lung masks were required as input data for CTVIPRO computation. For the convenience of clinical use with less input requirement and faster calculation speed, we proposed a simplified algorithm, in this study called VIAAVG. It only required AVG CT and the corresponding binary lung mask as input data to compute CTVIAVG:

$$\mathrm{CTVIAVG}(x) = \begin{cases} \frac{HU_{AVG}(x)}{-1000} \times \frac{HU_{AVG}(x)+1000}{1000} & \text{if} x \in L_{AVG} \\ 0 & \text{if} x \notin L_{AVG} \end{cases} \tag{6}$$

here $HU_{AVG}(x)$ and L_{AVG} were the HU value at voxel x and the binary lung mask defined on AVG CT, respectively.

2.11. Post-processing of CTVIs

In order to avoid the influence of no lung voxels, dot product between CTVI and 3D binary lung mask defined on T50 CT (whose volume was theoretically the smallest) was first performed. A 3D median filter was then applied to smooth noises and artifacts for each CTVI. For easy comparison, the filter applied was the same as in Kipritidis et al. study [18] within a cubic region of the dimension 7 × 7 × 7 voxels. Finally, VI-SPECT and each CTVI was normalized to the max voxel value and segmented into three equal volumes by the highest 1/3 value and lowest 1/3 value in lung, which represented high (H), medium (M) and low (L) function lung (FL) (i.e. HFL, MFL and LFL), respectively.

2.12. Accuracy assessment of VIAs

To assess the accuracy of each VIA, the similarity (i.e. spatial overlap) of each function lung between segmented VI-SPECT and each segmented CTVIs were quantified with the Dice Similarity Coefficient (DSC).

$$\mathrm{DSC} = \frac{2 \times \mathrm{FLV_{SPECT}} \cap \mathrm{FLV_{CTVI}}}{\mathrm{FLV_{SPECT}} + \mathrm{FLV_{CTVI}}} \tag{7}$$

where FLV_{SPECT} and FLV_{CTVI} were the corresponding segmented lung volumes (i.e. HFL, MFL and LFL, respectively) in VI-SPECT and CTVIs.

The average DSC for each CTVI was calculated and used as an index to evaluate the overall similarity between segmented VI-SPECT and segmented CTVIs.

$$\text{Average DSC} = \frac{DSC_{HFL} + DSC_{MFL} + DSC_{LFL}}{3} \tag{8}$$

We hypothesized that all CTVIs have the same similarity (i.e., accuracy) with the VI-SPECT. The average DSC values were compared one by one among four CTVIs using 2-tailed paired *t* test. The same cutoff values proposed by Yamamoto [31] were used to interpret DSC values: $0.8 < \mathrm{DSC} \leq 1.0$ as almost perfect, $0.6 < \mathrm{DSC} \leq 0.8$ as substantial, $0.4 < \mathrm{DSC} \leq 0.6$ as moderate, $0.2 < \mathrm{DSC} \leq 0.4$ as fair, $0.0 < \mathrm{DSC} \leq 0.2$ as slight.

The computation, post-processing, and qualitative accuracy assessment of CTVI were all performed in FLICT running on a workstation with dual-core Intel Xeon processors and 64 GB RAM. The total computation time for each CTVI was recorded and compared using 2-tailed paired *t* test.

3. Results

A visual comparison between different ventilation images is illustrates in Fig. 1 for a specific patient in transverse (first row) and coronal (second row) view. The correctness of segmentation algorithm used in this study can be confirmed by comparing the original VI-SPECT (first column) and the segmented VI-SPECT (second column). Generally, segmented CTVIPRO and CTVIAVG are very similar, and showing a high similarity with segmented VI-SPECT. However, the similarity between segmented CTVIJAC, as well as segmented CTVIHU, with segmented VI-SPECT seems poor, especially in the COPD region (middle lobe of right lung and lower lobe of left lung, indicated by yellow arrows).

Fig. 2 shows a box plot of DSC distribution for all CTVIs in different function lung regions. Castillo et al. [23] reported that, the highest correlation between VI-SPECT and CTVIHU and CTVIJAC lies within the lowest percentile range (1–20%).

In our study, the normality and the equality of error variances are found not good enough after Shapiro-Wilk's test of normality and Levene's test of equality of error variances. We have to use Dunnett T3 test, a non-parametric test, to analysis the relationship among VIAs, function lung regions and DSC values. We only find significant differences in DSC for CTVIJAC between function lung regions, with the LFL having the largest DSC comparing to two others ($p < 10^{-4}$). This is in agreement with the result of Castillo et al. However, for three other CTVIs (CTVIHU, CTVIPRO and CTVIAVG), MFL have the significantly smallest DSCs ($p < 10^{-4}$) while no significant difference in DSC are found between LFL and HFL. In addition, we find that there is a strong interaction between VIAs and function lung regions ($p < 10^{-4}$). The other key finding is that the DSC values are significantly different among different VIAs in the same function lung region. From large to small they are CTVIAVG, CTVIPRO, CTVIHU and CTVIJAC. The differences in DSC among different VIAs are also analyzed using the average DSC in all lung and explained in the following text.

The DSC values of each lung third for a specific enrolled patient are showed in Table 2. DSC values of CTVIPRO and CTVIAVG are nearly

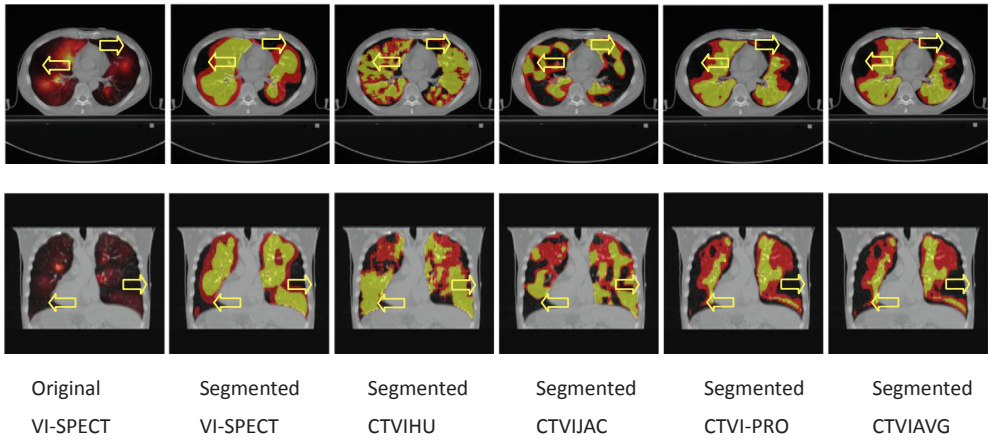

Fig. 1. Visual comparison between original VI-SPECT (first column), segmented VI-SPECT (second column), segmented CTVIHU (third column), segmented CTVIJAC (fourth column), segmented CTVIPRO (fifth column) and segmented CTVIAVG (sixth column) in transverse (first row) and coronal (second row) view. HFL, MFL and LFL are shown in yellow, red and black color in segmented VI-SPECT and CTVIs which masked by refined lung volume generated on T50 CT. All images in each row are on the same CT slice. COPD is observed in the middle lobe of left lung and lower lobe of right lung (indicated by the reported yellow arrow). (For interpretation of the references to colour in this figure legend, the reader is referred to the web version of this article.)

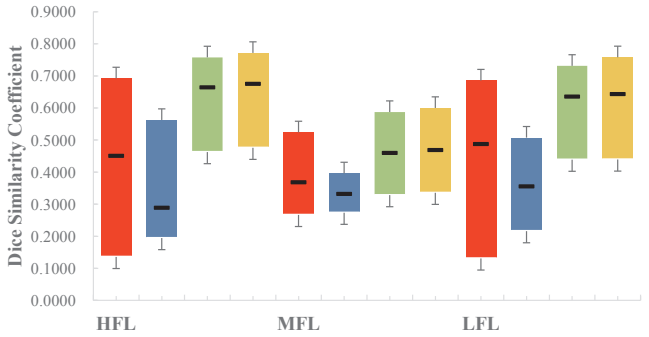

Fig. 2. The distribution of Dice similarity coefficient (DSC) between segmented VI-SPECT and each of CTVI (CTVIHU, CTVIJAC, CTVIPRO and CTVIAVG are shown in red, blue, green and orange, respectively) for high, medium and low function lung (HFL, MFL and LFL, respectively). The average DSC for each CTVI and each function lung region are marked as '-' in the figure. (For interpretation of the references to colour in this figure legend, the reader is referred to the web version of this article.)

Table 2
DSC values for each lung third between segmented VI-SPECT and CTVIs for a specific patient.

CTVI Algorithm	DSC			
	HFL	MFL	LFL	Average DSC
CTVIHU	0.5417	0.3807	0.5209	0.4811
CTVIJAC	0.2488	0.3317	0.2524	0.2776
CTVIPRO	0.6190	0.4505	0.6688	0.5795
CTVIAVG	0.6261	0.4575	0.6959	0.5932

substantial (~0.6), especially for the HFL and LFL, and obviously higher than those of CTVIHU and CTVIJAC. The DSC results for other patients have the similar pattern. The average DSC is the average of DSC values for HFL, MFL and LFL.

The distribution of average DSC of all patients for different CTVI is illustrated in Fig. 3. The mean of average DSC values are also reported in the figure. After 2-tailed paired *t* test one by one, the differences of average DSCs between each two algorithms are all significant ($p \leq 0.002$). From highest to lowest, the mean of average DSC values are 0.5958, 0.5865, 0.4465 and 0.3255 for segmented CTVIAVG, CTVIPRO, CTVIHU and CTVIJAC, respectively. Ventilation image generated by VIAAVG is much more similar to the clinical golden standard (VI-SPECT).

The total computation times (Fig. 4) for each CTVI are all generally less than 5 min. The null hypothesis is that all VIAs take the same

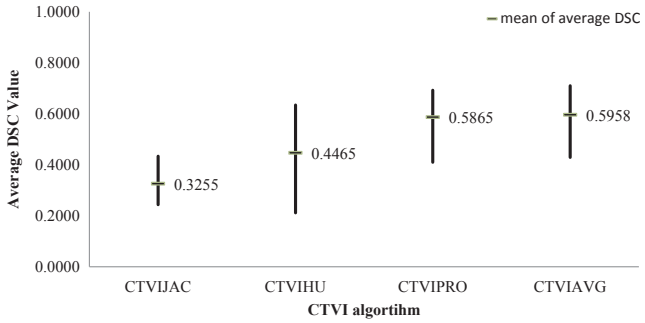

Fig. 3. The distribution of average DSC of all patients for different CTVIs. The mean of average DSC values are marked as '-' in the figure. ***P*** values derived from 2-tailed paired *t* test between each two segmented CTVIs are all less than 0.002.

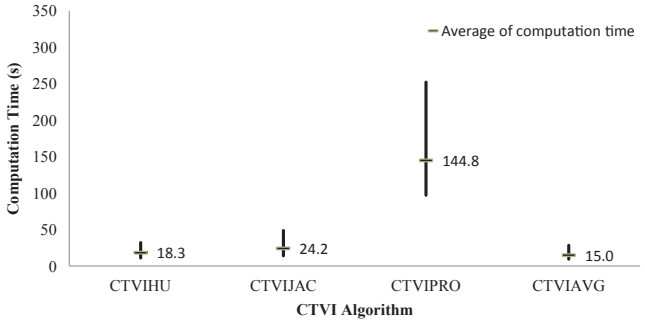

Fig. 4. The distribution of computation time of all patients for different CTVI. The mean of computation time were marked as '-' in the figure. ***P*** values derived from 2-tailed paired *t* test between each two segmented CTVIs were all less than 0.001.

computation time to generate CTVIs. However, after 2-tailed paired *t* test one by one, we find that the differences in computation time between each two VIAs are significant (***p*** less than 0.001). VIAPRO take a much longer computation time than other three VIAs, while the time for computing CTVI based on VIAAVG is the shortest with an average value of 15.0 s. The computation time of CTVIPRO distributes in a large range from 97.0 s to 252.0 s, since VIAPRO should process 10 phases 4DCT and much more sensitive with the slice number of each phase CT.

4. Discussion

In this study, we propose a simplified algorithm, VIAAVG, inspired by the method proposed by Kipritidis et al. with the aim to reduce input

requirement and computation time. In VIAHU and VIAJAC, two phases of 4DCT images (T50 and T00) are required as input data. In VIAPRO, even all phases of 4DCT images are required. In contrast, the simplified algorithm requires only AVG CT to compute CTVIAVG. The availability of this algorithm is evaluated by comparing its accuracy and efficiency with other three algorithms proposed for all enrolled patients. To the best of our knowledge, it is the largest patient cohort in this kind of studies. This makes our results more convincing in term of statistics with all p values no more than 0.002.

Segmented CTVIAVG shows significantly ($p \leq 0.002$) higher similarity with segmented VI-SPECT than other three CTVIs. The difference of the average DSC is large between VIAAVG and other two DIR-dependent VIAs, but marginal between VIAAVG and VIAPRO. No matter for lung cancer patient or esophageal cancer patient (with more or less probability of tumor obstruction, respectively), VIAPRO and VIAAVG, show nearly substantial correlation with VI-SPECT. The mean of average DSC values are 0.5812, 0.5928 and 0.5901, 0.5978, for lung cancer patients and esophageal cancer patients respectively. The accuracy of this simplified algorithm is at least not inferior to VIAs proposed before.

The simplified algorithm, VIAAVG, takes significantly less time to compute CTVI than other proposed algorithms. P values derived from 2-tailed paired t test between each two segmented CTVIs are all less than 0.001. Particularly, when compared to the second accurate algorithm, VIAPRO, the computation time is reduced by nearly 9 times since 10 phases matrices have to be processed for VIAPRO while only one matrix has to be processed for VIAAVG. Also it should be noted that the computation time recorded in this study is just the required time used for computing CTVIs when each input data is ready. The time spend on the pre-processing, such as deformable registration, CT image and DVF processing, lung volume contouring on relevant phase of 4DCT and converting the lung volume into mask are not included. If all times spend in the entire workflow are taken into account, the advantage of VIAAVG in computation time would be more obvious. Even with the help of artificial intelligence or deep learning in lung volume contouring, people have to take time to check the accuracy of the contours outlined automatically at the current state of art.

In addition, since our method only relies on the AVG CT, which is the preferred pCT in clinic when 4DCT was available [32], this makes the application of 4DCT-based ventilation image more convenient in clinical practice. For example, it is easy to collect the dose and lung function distribution parameters on the same AVG CT geometry to analysis the correlation between the dose-functional parameters and occurrence of radiotherapy induced complications, thereby avoiding the additional time and introduced errors by mapping function distribution onto the pCT.

VIAJAC only relies on the DVFs, which theoretically has ability to avoid the uncertainty from image noise and artifacts, but VIAJAC seems as the least accurate algorithm for CTVI generation in this study after 2-tailed paired t test one by one. The mean of average DSC of CTVIJAC is significantly lower (0.3255 vs. 0.4465, $p < 0.001$) even compared with other DIR-dependent VIA (VIAHU) in this study. Meanwhile, the mean of average DSC of two DIR-dependent VIAs (i.e., VIAHU and VIAJAC) are still lower compared with other two DIR-independent VIAs (i.e., VIAPRO and VIAAVG). Although these two results are respectively consistent with the key finding reported by Castillo et al. [23] and Kipritidis et al. [18], it is still difficult to give a definitive conclusion that DIR-dependent VIAs are inferior to the DIR-independent VIAs because different DIR algorithms and user-defined parameters employed may produce different DVF that favors the DIR-dependent CTVIs [31,28]. The effect of DIR errors on the spatial accuracy of DIR-dependent VIAs is the current research endeavor [27]. But it is still hard to make a clear conclusion even if the accuracy of DIR algorithm provided by the commercial software MIMvista has been evaluated and assessed equal to 0.6 voxel widths [33]. The stability or reproducibility of DIR-dependent CTVI should be pay more attention in the future works [34].

Kipritidis et al. [18] also reported that DIR-dependent VIAs appeared more accurate for visualizing tumor obstruction defect and abnormal lung voxels with HU > -600 or so [18]. However, we find an opposite result that VIAJAC and VIAHU would overestimate the lung function in clinical defect region (see the arrows in Fig. 1). This may be due to the following reasons: 1) the DIR algorithms used are different, and 2) the 4DCT scans in the study of Kipritidis et al. were also used for PET attenuation correction, while in this study 4DCT scans are acquired on a CT simulator. Our study provides 4DCT images with much higher quality and excludes the possibility of correlated image noise between 4DCT and VI-SPECT that favors the CTVIPRO or CTVIAVG.

5. Conclusion

The simplified algorithm proposed in this study, VIAAVG, shows a nearly substantial correlation with the commonly used clinic-gold-standard lung functional image (VI-SPECT). Compared with other proposed algorithms, it is a promising modality for the further application of 4DCT-based ventilation imaging in radiation therapy because of less input requirement, improved computation efficiency and independence on DIR.

Acknowledgements

The authors sincerely thank Dr. Li Mei and her team of the Nuclear Medicine Department of Peking TongRen Hospital for their great help in SPECT image acquisitions. This work was supported by the National Natural Science Foundation for Young Scholars of China (Grant No. 81502649) and National Key Projects of Research and Development (Grant No. 2016YFC0904600).

Appendix A. Supplementary data

Supplementary data to this article can be found online at https://doi.org/10.1016/j.ejmp.2019.08.006.

References

[1] Eslick EM, Stevens MJ, Bailey DL. SPECT V/Q in lung cancer radiotherapy planning. Semin Nucl Med 2019;49(1):31–6.
[2] Ireland RH, Tahir BA, Wild JM, et al. Functional image-guided radiotherapy planning for normal lung avoidance. Clin Oncol (R Coll Radiol) 2016;28(11):695–707.
[3] Yamamoto T, Kabus S, Klinder T, et al. Investigation of four-dimensional computed tomography-based pulmonary ventilation imaging in patients with emphysematous lung regions. Phys Med Biol 2011;56(7):2279–98.
[4] Ding K, Bayouth JE, Buatti JM, et al. 4DCT-based measurement of changes in pulmonary function following a course of radiation therapy. Med Phys 2010;37(3):1261–72.
[5] Latifi K, Feygelman V, Moros EG, et al. Normalization of ventilation data from 4D-CT to facilitate comparison between datasets acquired at different times. PLoS One 2013;8(12):e84083.
[6] King MT, Maxim PG, Diehn M, et al. Analysis of long-term 4-dimensional computed tomography regional ventilation after radiation therapy. Int J Radiat Oncol Biol Phys 2015;92(3):683–90.
[7] Kipritidis J, Hugo G, Weiss E, et al. Measuring interfraction and intrafraction lung function changes during radiation therapy using four-dimensional cone beam CT ventilation imaging. Med Phys 2015;42(3):1255–67.
[8] Yamamoto T, Kabus S, Bal M, et al. The first patient treatment of computed tomography ventilation functional image-guided radiotherapy for lung cancer. Radiother Oncol 2016;118(2):227–31.
[9] Kimura T, Doi Y, Nakashima T, et al. Combined ventilation and perfusion imaging correlates with the dosimetric parameters of radiation pneumonitis in radiation therapy planning for lung cancer. Int J Radiat Oncol Biol Phys 2015;93(4):778–87.
[10] Vinogradskiy Y, Castillo R, Castillo E, et al. Use of 4-dimensional computed tomography-based ventilation imaging to correlate lung dose and function with clinical outcomes. Int J Radiat Oncol Biol Phys 2013;86(2):366–71.
[11] Yaremko BP, Guerrero TM, Noyola-Martinez J, et al. Reduction of normal lung irradiation in locally advanced non-small-cell lung cancer patients, using ventilation images for functional avoidance. Int J Radiat Oncol Biol Phys 2007;68(2):562–71.
[12] Yamamoto T, Kabus S, von Berg J, et al. Impact of four-dimensional computed tomography pulmonary ventilation imaging-based functional avoidance for lung cancer radiotherapy. Int J Radiat Oncol Biol Phys 2011;79(1):279–88.
[13] Kimura T, Nishibuchi I, Murakami Y, et al. Functional image-guided radiotherapy planning in respiratory-gated intensity-modulated radiotherapy for lung cancer

patients with chronic obstructive pulmonary disease. Int J Radiat Oncol Biol Phys 2012;82(4):e663–70.
[14] Huang TC, Hsiao CY, Chien CR, et al. IMRT treatment plans and functional planning with functional lung imaging from 4D-CT for thoracic cancer patients. Radiat Oncol 2013;8:3.
[15] Kida S, Bal M, Kabus S, et al. CT ventilation functional image-based IMRT treatment plans are comparable to SPECT ventilation functional image-based plans. Radiother Oncol 2016;118(3):521–7.
[16] Guerrero T, Sanders K, Noyola-Martinez J, et al. Quantification of regional ventilation from treatment planning CT. Int J Radiat Oncol Biol Phys 2005;62(3):630–4.
[17] Reinhardt JM, Ding K, Cao K, et al. Registration-based estimates of local lung tissue expansion compared to xenon CT measures of specific ventilation. Med Image Anal 2008;12(6):752–63.
[18] Kipritidis J, Hofman MS, Siva S, et al. Estimating lung ventilation directly from 4D CT Hounsfield unit values. Med Phys 2016;43(1):33.
[19] Suga K. Technical and analytical advances in pulmonary ventilation SPECT with xenon-133 gas and Tc-99m-Technegas. Ann Nucl Med 2002;16(5):303–10.
[20] Callahan J, Hofman MS, Siva S, et al. High-resolution imaging of pulmonary ventilation and perfusion with 68Ga-VQ respiratory gated (4-D) PET/CT. Eur J Nucl Med Mol Imaging 2014;41(2):343–9.
[21] Kipritidis J, Siva S, Hofman MS, et al. Validating and improving CT ventilation imaging by correlating with ventilation 4D-PET/CT using 68Ga-labeled nanoparticles. Med Phys 2014;41(1):011910.
[22] Yamamoto T, Kabus S, Lorenz C, et al. Pulmonary ventilation imaging based on 4-dimensional computed tomography: comparison with pulmonary function tests and SPECT ventilation images. Int J Radiat Oncol Biol Phys 2014;90(2):414–22.
[23] Castillo R, Castillo E, Martinez J, et al. Ventilation from four-dimensional computed tomography: density versus Jacobian methods. Phys Med Biol 2010;55(16):4661–85.
[24] Kipritidis J, Tahir BA, Cazoulat G, et al. The VAMPIRE challenge: a multi-institutional validation study of CT ventilation imaging. Med Phys 2019;46(3):1198–217.
[25] Jensen KR, Brink C, Hansen O, et al. Ventilation measured on clinical 4D-CBCT: increased ventilation accuracy through improved image quality. Radiother Oncol 2017;125(3):459–63.
[26] Yamamoto T, Kabus S. Technical note: correction for the effect of breathing variations in CT pulmonary ventilation imaging. Med Phys 2018;45(1):322–7.
[27] Castillo R, Castillo E, Guerra R, et al. A framework for evaluation of deformable image registration spatial accuracy using large landmark point sets. Phys Med Biol 2009;54(7):1849–70.
[28] Fatyga M, Dogan N, Weiss E, et al. A voxel-by-voxel comparison of deformable vector fields obtained by three deformable image registration algorithms applied to 4DCT lung studies. Front Oncol 2015;5:17.
[29] Yamamoto T, Kabus S, Lorenz C, et al. 4D CT lung ventilation images are affected by the 4D CT sorting method. Med Phys 2013;40(10):101907.
[30] Pan T, Lee TY, Rietzel E, et al. 4D-CT imaging of a volume influenced by respiratory motion on multi-slice CT. Med Phys 2004;31(2):333–40.
[31] Yamamoto T, Kabus S, von Berg J, et al. Reproducibility of four-dimensional computed tomography-based lung ventilation imaging. Acad Radiol 2012;19(12):1554–65.
[32] Tian Y, Wang Z, Ge H, et al. Dosimetric comparison of treatment plans based on free breathing, maximum, and average intensity projection CTs for lung cancer SBRT. Med Phys 2012;39(5):2754–60.
[33] Markel D, Levesque I, Larkin J, et al. A 4D biomechanical lung phantom for joint segmentation/registration evaluation. Phys Med Biol 2016;61(19):7012–30.
[34] Castillo E, Castillo R, Vinogradskiy Y, et al. The numerical stability of transformation-based CT ventilation. Int J Comput Assist Radiol Surg 2017;12(4):569–80.